ResearchOnline@JCU

JAMES COOK UNIVERSITY AUSTRALIA

This is the author-created version of the following work:

Chalak Qazani, Mohamad Reza, Asadi, Houshyar, Mohamed, Shady, Lim, Chee Peng, and Nahavandi, Saeid (2022) ***An optimal washout filter for motion platform using neural network and fuzzy logic.*** **Engineering Applications of Artificial Intelligence, 108 .**

Access to this file is available from:

https://researchonline.jcu.edu.au/86743/

© 2021 Elsevier Ltd. All rights reserved. AAM available under a CC BY-NC-ND license.

Please refer to the original source for the final version of this work:

https://doi.org/10.1016/j.engappai.2021.104564

An Optimal Washout Filter for Motion Platform Using Neural Network and Fuzzy Logic

Mohammad Reza Chalak Qazani*,[a] Houshyar Asadi, [a] Shady Mohamed, [a] Chee Peng Lim, [a] Saeid Nahavandi [a]

[a]*The authors are with the Institute for Intelligent Systems Research and Innovation, Deakin University, Geelong, VIC 3125, Australia*

Abstract

To experience the motion sensation of a real vehicle through a motion simulator, a motion cueing algorithm (MCA) is required to transform the vehicle motions to the driving motion platform (DMP) while respecting the physical limitations of DMP. In this aspect, the optimal washout filter (WF) extracts the optimal motion signals including linear accelerations and angular velocities for the DMP with consideration of the human vestibular model and DMP motion states using the linear quadratic regulator (LQR) technique. The LQR technique is employed to obtain the optimal and pre-defined higher order transfer functions by solving the Riccati equation. However, the Riccati equation is solved using fixed weights, leading to an inconvenient usage of the DMP workspace. In this research, a new optimal WF model is designed and developed using a neural network (NN) and a fuzzy logic controller (FLC). The NN is introduced to solve the Riccati equation online while the FLC model is designed to extract the weighting matrices of the LQR technique. The proposed technique considers the physical DMP limitations online and reproduces accurate motion signals with a high degree of fidelity. The results demonstrate the efficiency of the developed optimal WF model as compared with those of existing optimal WF models.

Keywords: motion cueing algorithm, optimal washout filter, time-varying weights, fuzzy logic controller, Riccati equation, neural network.

1. Introduction

The parallel and serial robotic manipulators are useful to function as a driving motion platform (DMP) to regenerate up to 6 degree-of-freedom (6-DoF) motion signals [1, 2]. The usage of DMP are increasing in different fields such as biomedicine, transportation, and vehicular technology [3, 4]. An DMP is employed to regenerate the motion feeling for the user to experience virtual driving scenarios realistically. It is obvious that the DMP workspace is limited due to the physical constraints of the system [5-7]. As such, a motion cueing algorithm (MCA) is utilized to reproduce the motion cues that respect the physical DMP limitations. In this regard, the motion sickness as the main critical disadvantage of the MCA, which occurs when there is a discrepancy between the motion signals perceived via the visual and vestibular systems of an DMP user as compared with the motion signals experienced physically [8, 9]. The main source of this drawback is the physical DMP limitations and inappropriate MCA designs. Note that the human vestibular system is located inside the inner ear and it is composed of otolith organs and semicircular canals

* Corresponding author. Tel.: +61 411 859009; e-mail: m.r.chalakqazani@gmail.com.

to perceive the linear and angular motions, respectively.

The first MCA model was invented by Conrad and Schmidt [10], named as the classical washout filter (WF). A merging of the second-order high- and low-pass filters is employed in the classical WF structure to regenerate a sustainable linear acceleration motion sensation using somatogravic illusion [11]. Reid and Nahon had developed the classical WF for 6-DoF DMP because of the simplicity and easy tuning technique [12, 13]. Besides the simplicity of the classical WF model, there are some disadvantages associated with the classical WF, including fixed parameters, no cogitation of the human vestibular model, and the worst-case tuning technique. In order to eliminated the pre-mentioned shortcoming of the classical WF, adaptive WF is introduced [14]. The fuzzy logic controller (FLC) is used in designing the adaptive WF in order to vary the fixed terms of the classical WF [15-17] or regeneration of the motion compensation signal [18-20]. Kurosaki [21] exploited control techniques to minimize the motion error without taking into account the human vestibular system. Sivan et al. [22] introduced an optimal WF model using the linear quadratic regulator (LQR) technique regarding the human vestibular model. Nevertheless, Sivan et al. [22] chose the inappropriate control inputs, including angular displacement and linear acceleration, instead of the angular velocity and linear acceleration which were employed by Han et al. [23] and Telban and Cardullo [24] to increase the motion fidelity between the DMP user and the real vehicle driver. The usage of the angular displacement as an input motion signal was raised in Wu and Cardullo [25]. They [25] employed the angular and linear acceleration motion signals to increase the efficiency of the optimal WF model, leading to an increase in the motion states. This discovery, however, was before the work of Telban and Cardullo [24] on representation of the angular velocity as the best input motion signal. Chang et al. [26] proposed the real time optimal WF for 5-DoF motion scenario using 3-DoF DMP. Aminzadeh et al. [27] proposed the LQR-based optimal WF model with respect to the actuator limitations of a hexapod DMP system. Pham et al. [28] increased the efficiency of the optimal WF using a new tuning technique to reach the sickness-free simulation environment for the DMP user. Asadi et al. [29] developed a nonlinear optimal WF, adding the genetic algorithm inside the LQR technique to improve the motion fidelity while eliminating the drawbacks of the LQR technique, such as implementation of white noise and weight matrices. Asadi et al. [30] further proposed a robust optimal WF model using the genetic algorithm based on the physical DMP limitations to minimize the motion sensation error and maximize the sensation shape-following factor. Recently, Qazani et al. [31] proposed the optimal WF for the hexapod manipulator with consideration of the joints' limitations instead of the end-effector's limitation to increase the higher efficient usage of the workspace in regeneration of the high-fidelity motion signals for the user of the DMP compared with real vehicle's driver.

The LQR technique considers a dynamical model using linear differential equations and a cost function based on quadratic programming [32, 33]. The weight matrices of the states and inputs are defined in the quadratic programing procedure of LQR. The LQR technique is normally used to extract the feedback gains of a controller by solving a Riccati equation. It is critical to choose the weighting matrices of LQR appropriately subject to the problem in hand [34].

The incorporation of a neural network (NN) and FLC are used for predicting and solving the nonlinear complex plant models [35, 36]. Hui and Goh [37] used a combination of FLC and NN for retrieving the documents. Di et al. [38] proposed a highly efficient controller for an arc welding machine using FLC and NN. Baklouti et al. [39] introduced a type-2 FNN for better approximation of a complex system with better dealing with uncertainty. Antanasijević et al. [40] predicted the transition temperature of bent-core liquid crystals using FLC and general regression NN. Bas et al. [41] proposed a time series FLC using NN to specify the membership function for higher accurate estimation of the system.

The existing optimal WF models [21-24, 26-31] employ fixed weighting matrices, resulting in an inconvenient usage of the workspace and producing motion sickness through false motion cues. On the other hand, the low weighting matrices increases the chance of hitting the DMP workspace boundaries. The main contribution of this study is to develop a new optimal WF with efficient usage of the DMP workspace using time-varying weight optimal WF. The new optimal WF model is proposed to mitigate the

disadvantages of the existing optimal WF model using fixed weighting matrices [21-24, 26-31]. For this purpose, the Riccati equation is solved offline for a specific range of weighting matrices. The extracted feedback gains of LQR are used to train a neural network (NN) to identify the feedback gain matrices online inside the MCA model. In addition, fuzzy logic controllers (FLCs) are designed to extract the appropriate weighting matrices based on the current configuration of the DMP and the motion sensation error between the DMP user and the real vehicle driver. The main goal of this paper is to optimally use the DMP workspace and minimise the motion sensation error.

The existing optimal WF model with consideration of the human vestibular model is explained in the Section 2. The proposed optimal WF model using NN and FLC is illustrated in Section 3. The results are presented and discussed in Section 4, while the deduction is given in the last Section.

2. LQR-based Optimal WF Model

The optimal WF has the higher order optimal structure of the classical washout filter with consideration of the human vestibular model and DMP motion states to regenerate the optimal motion cues for the user of the DMP compared with the real vehicle driver. Therefore, the optimal WF is the combination of the human vestibular model, DMP motion states and the optimization solution. The human vestibular system is the main human sensory system to detect applied motions on body and the vestibular system mathematical models are developed [42] and used in different studies [22-24, 27, 29, 30]. The most accurate human vestibular model [24] is employed inside the optimal WF using LQR technique for extraction of the higher order filters with ability of regenerating high-fidelity motion cues for the user of the DMP. The structure of the optimal WF model is employed as a foundation of the proposed time-varying weight optimal WF model using FLC and NN in this paper.

2.1. Human Vestibular Model

The main part of the human motion perceptual system, known as human vestibular system, is composed of otolith organs and semicircular canals for perceiving the motion [43, 44]. It is the fastest biological system of the human body, which is situated inside the inner ears and is responsible of the postural stability and motion sensation. The otolith organs are responsible to perceive the translation motion, known as the sensed specific force. Telban and Cardullo [24] investigated different transfer function models pertaining to the otolith organs and identified the best mathematical model between the sensed specific force by the DMP user $\hat{f}$ and applied force f, as follows:

$$\frac{\hat{f}(s)}{f(s)} = K_{OTO}\left(\frac{(\tau_a s+1)}{(\tau_L s+1)(\tau_s s+1)}\right). \quad (1)$$

where τ_s, τ_a and K_{OTO} are 0.016 (s), 13.2 (s) and 0.4 along three-directions, and τ_L is 5.3 (s), 5.33 (s) and 5.33 (s) along x-, y- and z-directions, respectively. Additionally, Telban and Cardullo [24] introduced the semicircular model to connect the sensed angular velocity by the DMP user $\hat{\omega}$ and applied angular velocity ω, as follows:

$$\frac{\hat{\omega}}{\omega} = \left(\frac{\tau_1\tau_2 s^2}{(1+\tau_1 s)(1+\tau_2 s)}\right). \quad (2)$$

where τ_1 is 30 (s) in all three roll, pitch, and yaw angles, and τ_2 is 6.1 (s), 5.3 (s) and 10.2 (s) for the roll-, pitch- and yaw-angles, respectively.

The combination of Eqs. (1) and (2) produces a human vestibular model in state space mode as below:

$$\dot{\mathbf{x}}_{\mathrm{V}} = \mathbf{A}_{\mathrm{V}}\mathbf{x}_{\mathrm{V}} + \mathbf{B}_{\mathrm{V}}\mathbf{u}. \quad (3.a)$$

$$\hat{\mathbf{y}}_{\mathrm{V}} = \mathbf{C}_{\mathrm{V}}\mathbf{x}_{\mathrm{V}} + \mathbf{D}_{\mathrm{V}}\mathbf{u}. \quad (3.b)$$

where $\mathbf{A_v}$, $\mathbf{B_v}$, $\mathbf{C_v}$ and $\mathbf{D_v}$ are the state space matrices of the human vestibular model in longitudinal and lateral channels, i.e.:

$$\mathbf{A_v} = \begin{bmatrix} \mathbf{A_{SCC}} & \mathbf{0} \\ \mathbf{0} & \mathbf{A_{OTO}} \end{bmatrix}, \mathbf{B_v} = \begin{bmatrix} \mathbf{B_{SCC}} \\ \mathbf{B_{OTO}} \end{bmatrix} \quad (4.a)$$

$$\mathbf{C_v} = \begin{bmatrix} \mathbf{C_{SCC}} & \mathbf{0} \\ \mathbf{0} & \mathbf{C_{OTO}} \end{bmatrix}, \mathbf{D_v} = \begin{bmatrix} \mathbf{D_{SCC}} \\ \mathbf{D_{OTO}} \end{bmatrix} \quad (4.b)$$

where **SCC** and **OTO** refer to the semicircular canals and otolith organs of the human vestibular system, respectively. It should note that there is no semicircular model in the heave channel, and no otolith model in the yaw channel. In addition, $\mathbf{u}$ and $\hat{\mathbf{y}}_{\mathbf{v}}$ are the input and output vectors in the longitudinal channel, i.e.:

$$\mathbf{u} = \left[\dot{\theta}, \ddot{\mathrm{PCP}}_x\right]^{\mathrm{T}}, \hat{\mathbf{y}}_{\mathbf{v}} = \left[\hat{\dot{\theta}}, \widehat{\ddot{\mathrm{PCP}}_x}\right]^{\mathrm{T}} \quad (5)$$

and in the lateral channel:

$$\mathbf{u} = \left[\dot{\phi}, \ddot{\mathrm{PCP}}_y\right]^{\mathrm{T}}, \hat{\mathbf{y}}_{\mathbf{v}} = \left[\hat{\dot{\phi}}, \widehat{\ddot{\mathrm{PCP}}_y}\right]^{\mathrm{T}} \quad (6)$$

and in the heave channel:

$$\mathbf{u} = \left[\ddot{\mathrm{PCP}}_z\right]^{\mathrm{T}}, \hat{\mathbf{y}}_{\mathbf{v}} = \left[\widehat{\ddot{\mathrm{PCP}}_z}\right]^{\mathrm{T}} \quad (7)$$

and in the yaw channel:

$$\mathbf{u} = \left[\dot{\psi}\right]^{\mathrm{T}}, \hat{\mathbf{y}}_{\mathbf{v}} = \left[\hat{\dot{\psi}}\right]^{\mathrm{T}} \quad (8)$$

2.2. Riccati Equation Solution

Fig. 1.a shows a schematic flowchart of the existing optimal WF model with the human vestibular model, aiming to reduce the motion sensation error between the DMP user and the real vehicle driver. The purpose of the existing optimal WF model is to identify the optimal transfer function, $\mathbf{W}(\boldsymbol{s})$, that can be utilized to calculate the motion input signal of the DMP, $\mathbf{u_s}$ regarding the motion input signal of the real vehicle user, $\mathbf{u_A}$, as follows:

$$\mathbf{u_s}(\boldsymbol{s}) = \mathbf{W}(\boldsymbol{s}) \times \mathbf{u_A}(\boldsymbol{s}) \quad (9)$$

Fig. 1.b illustrates the structure of the optimal WF model along the longitudinal channel, which consists of the translational, rotational and tilt coordination channels. The input motion signals (linear acceleration and angular velocity) are scaled down and limited, in order to keep the DMP inside the workspace constraints. The double and single integrations are added to the end of both the translational and rotation channels to calculate the translational and angular positions of the DMP. The three higher degree transfer functions, $\mathbf{W_{11}}$, $\mathbf{W_{12}}$ and $\mathbf{W_{22}}$ which are used to filter the motion signals, are the entries of the $\mathbf{W}(\boldsymbol{s})$ matrix.

The motion sensation error between the DMP user and the vehicle driver based on Fig. 1.a and Eq. (4) can be found:

$$\dot{\mathbf{x}}_{\boldsymbol{e}} = \mathbf{A_v}\mathbf{x}_{\boldsymbol{e}} + \mathbf{B_v}\mathbf{u_s} - \mathbf{B_v}\mathbf{u_A} \quad (10.a)$$

$$\boldsymbol{e} = \mathbf{C_v}\mathbf{x}_{\boldsymbol{e}} + \mathbf{D_v}\mathbf{u_s} - \mathbf{D_v}\mathbf{u_A} \quad (10.b)$$

where $\boldsymbol{e}$ and $\mathbf{x}_{\boldsymbol{e}}$ are the human sensation error and vestibular states error, i.e., $\mathbf{x}_{\boldsymbol{e}} = \mathbf{x}_{\boldsymbol{s}} - \mathbf{x_A}$, while $\mathbf{x_s}$ and

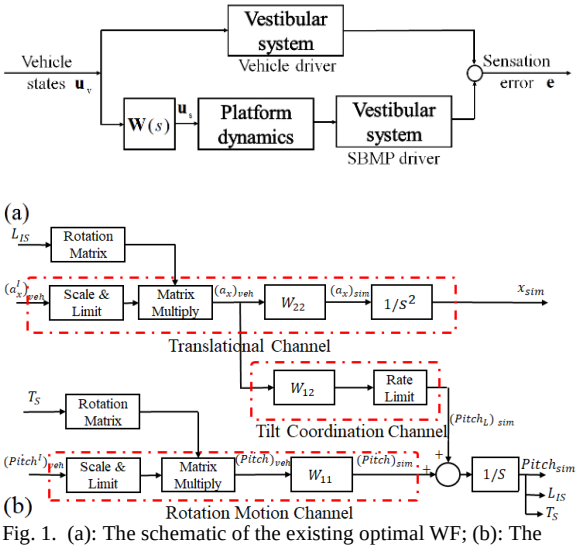


Fig. 1. (a): The schematic of the existing optimal WF; (b): The block diagram of the existing optimal WF along longitudinal channel.

$\mathbf{x_A}$ are the vestibular states of the DMP user and the real vehicle driver.

The input motion signal should be added to the state space model of Eq. (9), in order to extract the motion sensation error between the DMP user and the real vehicle driver. The input motion signal of the real vehicle driver is white noise in the state space model as:

$$\dot{\mathbf{x}}_{\mathbf{n}} = \mathbf{A_n}\mathbf{x_n} + \mathbf{B_n}\mathbf{w} \quad (11.a)$$

$$\mathbf{u_A} = \mathbf{x_n} \quad (11.b)$$

where $\mathbf{w}$ and $\mathbf{x_n}$ are white noise and the filtered white noise by the appropriately chosen matrices as $\mathbf{A_n}$ and $\mathbf{B_n}$.

All serial and parallel DMP systems have a restricted workspace because of their physical limitations. The DMP limitations in the Cartesian coordinate space are the linear and angular displacement and velocity. To extract the linear and angular motion and velocity, $\mathbf{x_d}$ should be cogitated inside the model as:

$$\dot{\mathbf{x}}_{\mathbf{d}} = \mathbf{A_d}\mathbf{x_d} + \mathbf{B_d}\mathbf{u_s} \quad (12)$$

where $\mathbf{A_d}$, $\mathbf{B_d}$ and $\mathbf{x_d}$ are for the longitudinal channel as:

$$\mathbf{A_{d,Longitudinal}} = \begin{bmatrix} 0 & 1 & 0 & 0 \\ 0 & 0 & 1 & 0 \\ 0 & 0 & 0 & 0 \\ 0 & 0 & 0 & 0 \end{bmatrix} \quad (13.a)$$

$$\mathbf{B_{d,Longitudinal}} = \begin{bmatrix} 0 & 0 \\ 0 & 0 \\ 0 & 1 \\ 1 & 0 \end{bmatrix} \quad (13.b)$$

$$\mathbf{x_{d,Longitudinal}} = [\iiint a_x dt^3 \quad \iint a_x dt^2 \quad \int a_x dt \quad \theta]^{\mathrm{T}} \quad (13.c)$$

and for the lateral channel:

$$\mathbf{A_{d,Lateral}} = \begin{bmatrix} 0 & 1 & 0 & 0 \\ 0 & 0 & 1 & 0 \\ 0 & 0 & 0 & 0 \\ 0 & 0 & 0 & 0 \end{bmatrix} \quad (14.a)$$

$$\mathbf{B_{d,Lateral}} = \begin{bmatrix} 0 & 0 \\ 0 & 0 \\ 0 & 1 \\ 1 & 0 \end{bmatrix} \quad (14.b)$$

$$\mathbf{x_{d,Lateral}} = \left[\iiint a_y dt^3 \quad \iint a_y dt^2 \quad \int a_y dt \quad \varphi\right]^{\mathrm{T}} \quad (14.c)$$

and for the heave channel:

$$\mathbf{A_{d,Heave}} = \begin{bmatrix} 0 & 1 & 0 \\ 0 & 0 & 1 \\ 0 & 0 & 0 \end{bmatrix} \quad (15.a)$$

$$\mathbf{B_{d,Heave}} = \begin{bmatrix} 0 \\ 0 \\ 1 \end{bmatrix} \quad (15.b)$$

$$\mathbf{x_{d,Heave}} = [\iiint a_z dt^3 \quad \iint a_z dt^2 \quad \int a_z dt]^{\mathrm{T}} \quad (15.c)$$

and for the yaw channel:

$$\mathbf{A_{d,Yaw}} = \begin{bmatrix} 0 & 1 \\ 0 & 0 \end{bmatrix} \quad (16.a)$$

$$\mathbf{B_{d,Yaw}} = \begin{bmatrix} 0 \\ 1 \end{bmatrix} \quad (16.b)$$

$$\mathbf{x_{d,Yaw}} = [\int \psi dt \quad \psi]^{\mathrm{T}} \quad (16.c)$$

It is critical to washout the DMP's end-effector to the neutral position to reproduce the motion cue while keeping the end-effector inside the workspace boundaries [24, 30]. The integral of the translation movement is added to Eqs. (13) to (16). Eqs. (9) to (12) are combined to obtain the final state space model as:

$$\dot{\mathbf{x}} = \mathbf{A}\mathbf{x} + \mathbf{B}\mathbf{u_s} + \mathbf{H}\mathbf{w} \quad (17.a)$$

$$\mathbf{y} = [\boldsymbol{e} \quad \mathbf{x_d}]^{\mathbf{T}} = \mathbf{C}\mathbf{x} + \mathbf{D}\mathbf{u_s} \quad (17.b)$$

where **A**, **B**, **C**, **D**, **H** and **x** are:

$$\mathbf{A} = \begin{bmatrix} \mathbf{A_v} & \mathbf{0} & -\mathbf{B_v} \\ \mathbf{0} & \mathbf{A_d} & \mathbf{0} \\ \mathbf{0} & \mathbf{0} & \mathbf{A_n} \end{bmatrix}, \mathbf{B} = \begin{bmatrix} \mathbf{B_v} \\ \mathbf{B_d} \\ \mathbf{0} \end{bmatrix} \quad (18.a)$$

$$\mathbf{C} = \begin{bmatrix} \mathbf{C_v} & \mathbf{0} & -\mathbf{D_v} \\ \mathbf{0} & \mathbf{I} & \mathbf{0} \end{bmatrix}, \mathbf{D} = \begin{bmatrix} \mathbf{D_v} \\ \mathbf{0} \end{bmatrix} \quad (18.b)$$

$$\mathbf{H} = \begin{bmatrix} \mathbf{0} \\ \mathbf{0} \\ \mathbf{B_n} \end{bmatrix}, \mathbf{x} = [\mathbf{x}_{\boldsymbol{e}} \quad \mathbf{x_d} \quad \mathbf{x_n}]^{\mathbf{T}} \quad (18.c)$$

The cost function over the time period of t_0 to t_1 for the optimal WF model using LQR technique can be formulated as:

$$J = E\left\{\int_{t_0}^{t_1} \left(\mathbf{e}^{\mathrm{T}}\mathbf{Q}\mathbf{e} + \mathbf{x_d^{\mathrm{T}}}\mathbf{R_d}\mathbf{x_d} + \mathbf{u_s^{\mathrm{T}}}\mathbf{R}\mathbf{u_s}\right) dt\right\} \quad (19)$$

where **Q**, $\mathbf{R_d}$ and **R** are the weighing parameters used to penalize the outputs, including the sensed angular and linear motions, extra terms, including the angular and linear motions, and input signals, including rotational and translational motions signals. Note that **Q** and $\mathbf{R_d}$ are positive semi definite matrices and **R** is a positive definite matrix. In addition, **Q**, $\mathbf{R_d}$ and **R** should be chosen properly, in order to obtain suitable results with respect to the DMP limitations. The physical limitations of a hexapod DMP system, which is employed in this study, is presented in Table I. Eqs. (17) and (19) are transformed into the standard form of the optimal control as:

$$\dot{\mathbf{x}} = \mathbf{A}'\mathbf{x} + \mathbf{B}\mathbf{u}' + \mathbf{H}\mathbf{w} \quad (20.a)$$

$$J' = E\left\{\int_{t_0}^{t_1} (\mathbf{x}^{\mathrm{T}}\mathbf{R_1'}\mathbf{x} + \mathbf{u}'\mathbf{R_2}\mathbf{u}')dt\right\} \quad (20.b)$$

where $\mathbf{A}'$, $\mathbf{u}'$, $\mathbf{R_1'}$ and $\mathbf{R_2}$ are:

$$\mathbf{G} = \mathrm{diag}[\mathbf{Q} \quad \mathbf{R_d}], \mathbf{L} = \mathbf{C}^{\mathrm{T}}\mathbf{G}\mathbf{C}, \mathbf{M} = \mathbf{C}^{\mathrm{T}}\mathbf{G}\mathbf{D} \quad (21.a)$$

$$\mathbf{R_2} = \mathbf{R} + \mathbf{D}^{\mathrm{T}}\mathbf{G}\mathbf{D}, \mathbf{R_1'} = \mathbf{L} - \mathbf{M}\mathbf{R_2^{-1}}\mathbf{M}^{\mathrm{T}} \quad (21.b)$$

$$\mathbf{A}' = \mathbf{A} - \mathbf{B}\mathbf{R_2^{-1}}\mathbf{M}^{\mathrm{T}}, \mathbf{u}' = \mathbf{u_s} + \mathbf{R_2^{-1}}\mathbf{M}^{\mathrm{T}}\mathbf{x} \quad (21.c)$$

Eq. (19) is minimised when the input signal $\mathbf{u}'$ is:

TABLE I
THE CONSTRAINTS OF THE HEXAPOD DMP

Index	Position	Velocity	Acceleration
x	±0.6 (m)	±1.2 (m/s)	±3.2 (m/s²)
y	±0.6 (m)	±1.2 (m/s)	±3.6 (m/s²)
z	±0.2 (m)	±0.95 (m/s)	±4.8 (m/s²)
Roll	±20 (d)	±112 (d/s)	±600 (d/s²)
Pitch	±20 (d)	±62 (d/s)	±600 (d/s²)
Yaw	±25 (d)	±61 (d/s)	±240 (d/s²)

m: meter; d: degree; s: second;

$$\mathbf{u}' = -\mathbf{R_2^{-1}}\mathbf{B}^{\mathrm{T}}\mathbf{P}\mathbf{x} \tag{22}$$

P can be extracted by solving the Riccati equation as:

$$\mathbf{u}' = -\mathbf{R_2^{-1}}\mathbf{B}^{\mathrm{T}}\mathbf{P}\mathbf{x} \tag{23}$$

The MATLAB function "care" is employed to obtain the **P** matrix. The feedback gain matrix of the LQR-based optimal control can be extracted as follows:

$$\mathbf{K} = \mathbf{R_2^{-1}}(\mathbf{B}^{\mathrm{T}}\mathbf{P} + \mathbf{M}^{\mathrm{T}}) \tag{24}$$

The extracted **K** matrix is employed to find $\mathbf{W}(\boldsymbol{s})$ as the optimal transfer function matrix based on Telban and Cardullo [24]. The elements of $\mathbf{W}(\boldsymbol{s})$ are the higher order transfer functions of the optimal WF model shown in Fig. 1.b.

3. Proposed Adaptive Fuzzy-based Optimal WF

The first part of this Section presents the online LQR solver to find the feedback gain matrix using a NN model. The second part describes an FLC model to extract the suitable weighting matrices based on the current DMP situation.

3.1. Online Riccati Equation Solver Using NN

The NN model employs a learning process that imitates the biological neural network of the brain using mathematical formulation [45-48]. NN is very popular in different fields such as controller [49, 50], forecasting [51, 52] and medical [53]. The output of the j^{th} neuron in the i^{th} layer can be calculated as:

$$h_j^i = f\left(g_j^i\right) \tag{25}$$

where f and h are the activation function and weighted input respectively, while

$$g_j^i = \sum_{k=1}^{r+1} \mathrm{W}_{k,j}^i \, h_k^{i-1} \tag{26}$$

where $\mathrm{W}_{k,j}^i$ is the connection weight from the k^{th} output of the previous layer to the j^{th} output of the current layer, and h_k^{i-1} is the previous layer output. The last outputs of each layer equal to one, i.e., $h_{r+1}^i = 1$.

To solve the cost function in Eq. (20) using the Riccati equation, the MATLAB "care" function is employed to find the feedback gain matrix of the LQR-based optimal control. The Riccati equation cannot be solved online owing to a computational load. As such, the Riccati equation is solved offline based on different weighting matrices. The ranges of the weighting parameters are selected based on the physical DMP limitations. The back-propagation technique [54, 55] is applied to a NN model with three layers including input, hidden, and output as per conducted study in [56]. The number of neurons in a hidden layer is 100 which is chosen using trial-and-error approach in order to reach the best possible solution with less means square error (MSE). The hyperbolic tangent with a zero centre is selected because it is suitable for the training process [57]. A data set of 1600000 samples is extracted by solving the Riccati equation offline. The data set is used to train the NN model to yield the feedback gain matrices.

3.2. Proposed Fuzzy Logic Control Unit

Fig 3. a-b depict the structure of the proposed optimal WF model using NN and FLC, and the state space model of the proposed optimal WF model in the longitudinal channel. The proposed method can be used to develop the model along lateral, heave and yaw channels. The MATLAB function of "optimal state space model" is used to extract the optimal state space matrices based on the extracted feedback gain matrices via the NN model (Fig. 2.a). Then, the extracted optimal matrices are used inside the state space model shown in Fig. 2.b to extract the optimal motion signal of the DMP when the motion signals of the real vehicle are used as the inputs of the model.

The inputs of the fuzzy logic units along the longitudinal channel are the current linear position, linear velocity, angular position, error of sensed

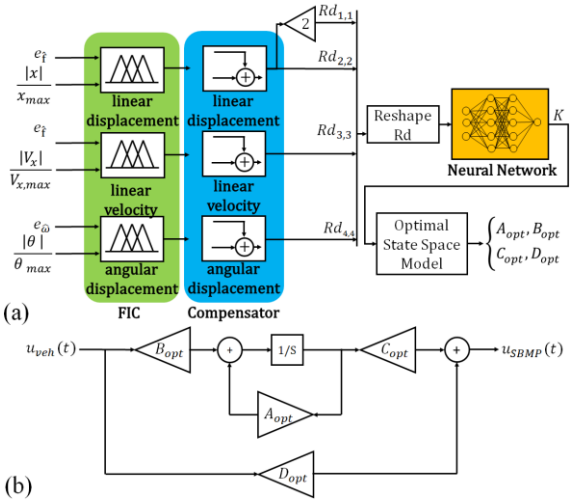


Fig. 2. (a): The structure of the proposed optimal WF using NN and FLC; (b): The state space model of the proposed optimal WF.

angular velocity and sensed specific force between the DMP user and the vehicle driver. The first inputs of the fuzzy units are normalised based on the human threshold unit for sensing the translational and rotational movement via the human vestibular system. The second inputs of the fuzzy units are normalize based on the physical DMP limitations, as shown in Table I. The human body cannot detect the size of the motion. Indeed, the human vestibular system can perceive the motion in small, medium, or large ranges in various channels such as longitudinal. Then, the FLC model to categorise the signals into five groups (massive positive, positive, zero, negative, and massive negative), in order to simulate the human vestibular system. The current position of the DMP as a second input of the FLC model can be divided into five different groups (massive near, near, medium, far and massive far), in order to indicate the current DMP situation. The compensator units are added in parallel to the FLC units, in order to detect the motion direction of the DMP and update the weighting parameters of the LQR technique. As an example, if the end-effector is close to the limitation while moving towards the neutral position in the next step, the compensator unit decreases the corresponding weighting parameter, to produce a better outcome with a convenient usage of the workspace. The fuzzy control actions are imposed to the weighting parameters of the LQR technique, and they are classified in five portions (massive big, big,

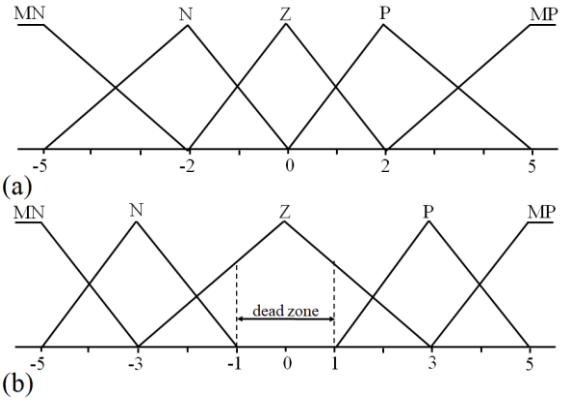


Fig. 3. The membership functions: (a): translational sensation error; (b): rotational sensation error.

medium, small and massive small). The fuzzy control efforts are normalised regarding the physical DMP limitations.

3.3. Membership Functions and Rules

Fig. 3. a-b display the membership functions for the first inputs of the fuzzy units, including the linear displacement, linear velocity and angular displacement. The triangular membership function is employed because it has a low computational load and it is easy to define with a small number of data samples. The motion sensation errors are normalised by dividing to the human threshold unit pertaining to sensing the angular velocity (5 degree/s) and linear acceleration signal (0.17 m/s^2) based on Telban and Cardullo [24]. The difference between two membership functions in Fig. 3. a-b is because of the structure of the semicircular canals and otolith organs [24]. The semicircular canals is not able to detect the rotational motion signal under the human threshold unit, as the driver cannot feel the angular motion [24]. Fig. 4 and Fig. 5 depict the membership functions of the second inputs of the FLC units and the fuzzy control action, respectively. The second input of the FLC units are linear displacement, linear velocity, and angular displacement of the DMP end-effector. As the main motivation of this method is the high-efficient usage of the DMP workspace boundaries, these parameters are considered as the second input of FLC units to calculate the appropriate weighting parameters based on the current configuration of the end-effector.

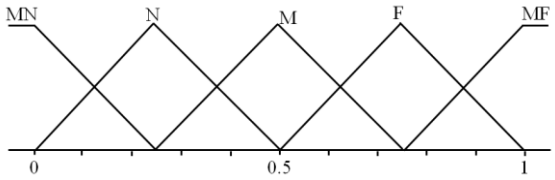


Fig. 4. The membership functions of the linear displacement, linear velocity and angular displacement inputs.

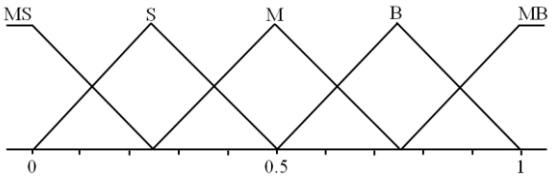


Fig. 5. The membership functions of fuzzy control actions including the weighting matrices of linear displacement, linear velocity and angular displacement.

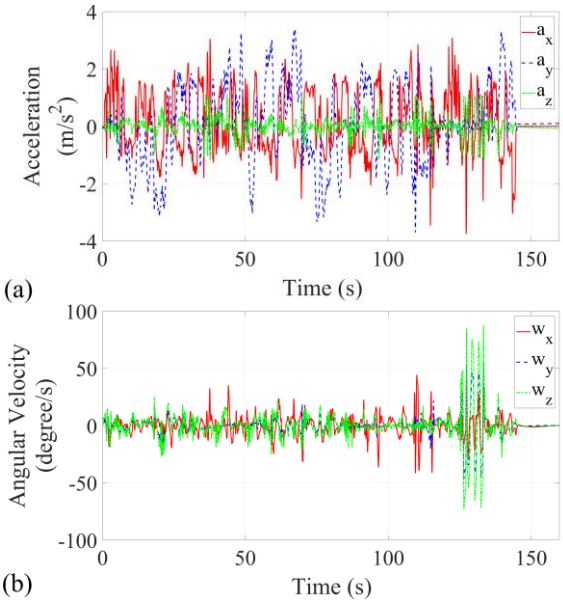


Fig. 6. The motion signal of the real vehicle for 150 seconds: (a) linear acceleration; (b) angular velocity.

These parameters are calculated via dividing the linear and angular motion indexes of the end-effector to its corresponding limitations. The parameter can vary from zero to one, while zero indicates the more available displacement area for the end-effector, and 1 means the end-effector is very close to the workspace boundaries.

The output membership functions of the linear displacement unit are calculated as:

$$\mu_{MS}(x;0,0.25) = \max\left(\min\left(\frac{-0.25-x}{0.25},1\right),0\right) \quad (27)$$

$$\mu_{S}(x;0,0.25,0.5) = \max\left(\min\left(\frac{x}{0.25},\frac{0.5-x}{0.25}\right),0\right) \quad (28)$$

$$\mu_{M}(x;0.25,0.5,0.75) = \max\left(\min\left(\frac{x-0.25}{0.25},\frac{0.75-x}{0.25}\right),0\right) \quad (29)$$

$$\mu_{M}(x;0.5,0.75,1) = \max\left(\min\left(\frac{x-0.5}{0.25},\frac{1-x}{0.25}\right),0\right) \quad (30)$$

$$\mu_{M}(x;0.75,1) = \max\left(\min\left(\frac{x-0.75}{0.25},1\right),0\right) \quad (31)$$

Table II presents the asymmetric rules of the proposed FLC model, which are based on the Mamdani-type fuzzy control scheme. The translational motion sensation error and the

TABLE II
FUZZY CONTROL RULES FOR LINEAR DISPLACEMENT CHANNEL

W_x		$e_{\dot{f}_x}$ MN	N	Z	P	MP
$\frac{x}{\max\{x\}}$	MN	MS	MS	MS	MS	MS
	N	MS	S	S	S	MS
	M	S	M	M	M	S
	F	M	B	B	B	M
	MF	B	MB	MB	MB	B

MN: massive negative and massive near; N: negative and near; Z: zero; P: positive; MP: massive positive; M: middle and medium; F: far; MF: massive far; MS: massive small; S: small; B: big; MB: massive big.

TABLE III
THE RESULT OF THE TIME-INVARIANT AND TIME-VARYING OPTIMAL WFS.

Index	RMSE			CC		
	CL	EX	PR	CL	EX	PR
SAV ω_Θ	0.148	0.120	0.117	0.290	0.582	0.673
SAV ω_ϕ	0.171	0.096	0.104	0.219	0.840	0.788
SAV ω_ψ	0.180	0.094	0.090	0.6323	0.948	0.955
SSF a_x	1.010	0.659	0.564	0.481	0.929	0.935
SSF a_y	1.232	0.786	0.710	0.414	0.936	0.931
SSF a_z	0.2972	0.282	0.250	0.235	0.403	0.504

SAV: Sensed Angular Velocity; SSF: Sensed Specific Force; RMSE: Root Mean Square Error; CC: Correlation Coefficient; EX: Existing; CL: Classical; Pr: Proposed.

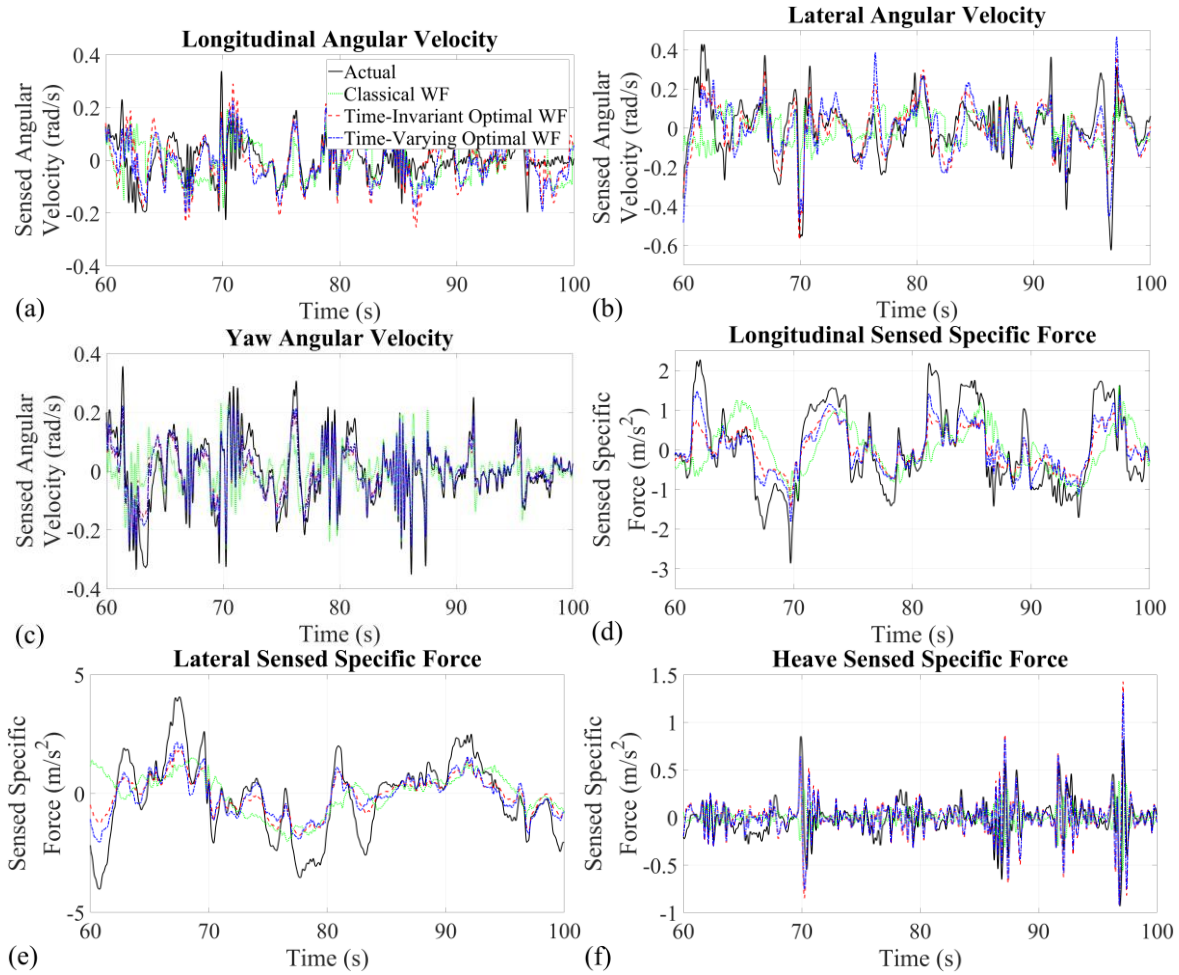


Fig. 7. The sensed angular velocity and specific force for the existing and proposed optimal WF models along: (a) rotational mode of longitudinal channel (b) rotational mode of lateral channel (c) rotational mode of vertical channel (d) translational mode of longitudinal channel (e) translational mode of lateral channel (f) translational mode of vertical channel.

translational position of the end-effector are the inputs of the rule table. They are used to decide the fuzzy control actions, namely the weighting parameters. The same methodology can be used to define the rule table for the linear velocity and rotational position FLC units, as all three have the same influence in the DMP displacement. The fuzzy control actions are generated based on the fuzzy rules. As an example, a high motion sensation error and a very near DMP position generates a very small weighting parameter, which is not to penalise the linear motion very restrictedly.

4. Results and Discussion

The effectiveness of the proposed time-varying weight optimal WF is compared with classical WF, which is proposed by Conrad and Schmidt [10], and with LQR-based time-invariant weight optimal WF proposed by Telban and Cardullo [24] (existing optimal WF). The three investigated methods are implemented in the Simulink environment of MATLAB. The role of the MCA unit is to regenerate the motion signals and keep the DMP inside the

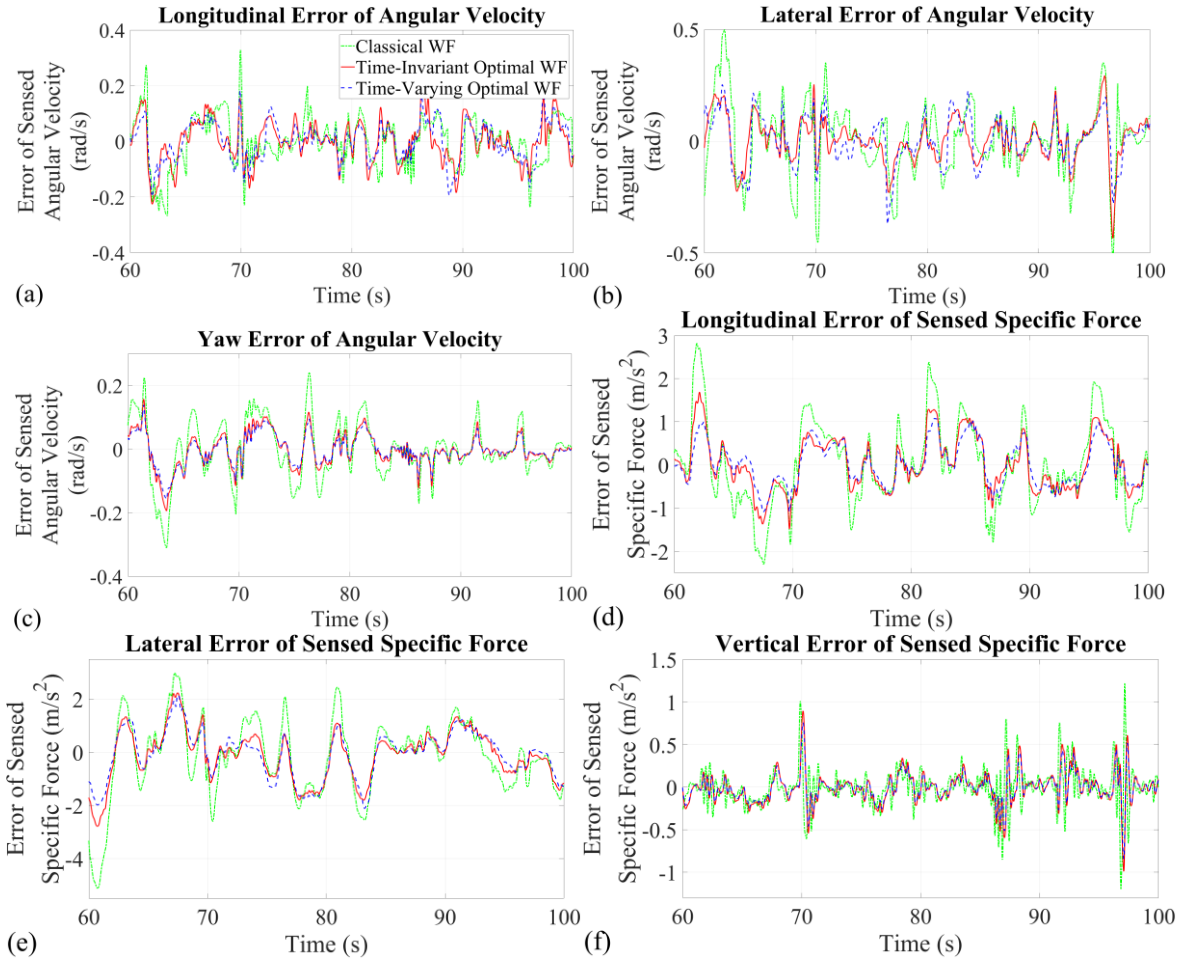


Fig. 8. The errors of the sensed angular velocity and specific force for the existing and proposed optimal WF models along: (a) rotational mode of longitudinal channel (b) rotational mode of lateral channel (c) rotational mode of vertical channel (d) translational mode of longitudinal channel (e) translational mode of lateral channel (f) translational mode of vertical channel.

workspace limitations, as well as provide the same motion sensation for the DMP user as experienced by the vehicle driver. The proposed optimal WF model is feasible, owing to the online Riccati equation solver with the NN model. In addition, both the existing and proposed optimal WF models are tuned to respect the workspace limitations. It should note that the same scaling factors are implemented for both techniques to reach a fair comparison, as follows:

$$\text{Scall}\{a_x, a_y, a_z\} = [1/3 \quad 1/3 \quad 1] \tag{32.a}$$

$$\text{Scall}\{\dot{\phi}, \dot{\theta}, \dot{\psi}\} = [1 \quad 1 \quad 1/5] \tag{32.b}$$

The input motion signals (angular velocity and linear acceleration) validate the proposed optimal WF model as compared with the existing classical and optimal WF models are extracted using the Rigs of Rods application (version 0.39.5) for four channels, as depicted in Fig. 6.a-b after scaling via Eq. (31) for a duration of 160 seconds. Besides that, two different procedures are taken to validate the regenerated motion signals of the proposed optimal WF model as compared with those of the existing optimal WF model, namely the root mean square error (RMSE) and correlation coefficient (CC). The RMSE calculation of the rotational and translational sensation between the vehicle driver and the DMP user is straightforward. A higher RMSE score indicates a more inconvenient

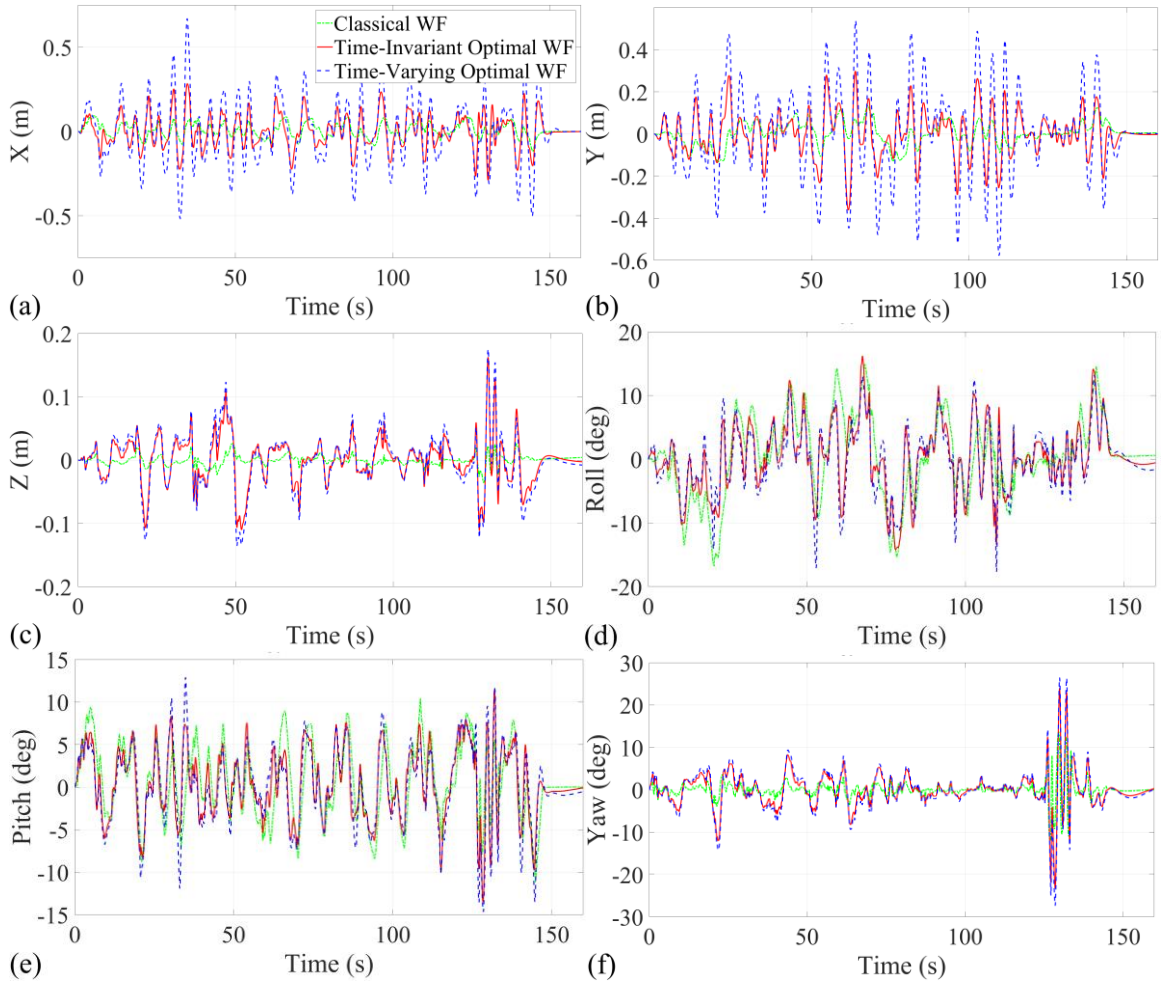


Fig. 9. Linear and angular movement of the DMP using time-invariant and time-varying optimal WF models: (a) *x*-axis; (b) *y*-axis; (c) z-axis; (d) *roll*-axis; (e) *pitch*-axis; (f) *yaw*-axis.

usage of the workspace boundaries. Also, generating false motion cues can cause motion sickness or artefact, which is the biggest drawback of the MCA model. But, the RMSE alone cannot validate the MCA model accurately, as the human vestibular model cannot perceive the motion signal quantitatively. As such, the CC score has been employed in Asadi et al. [30] to validate the regenerated motion signal via the MCA model. A higher CC score indicates a better shape-following capability of the reference motion signal for the DMP user as compared with those from the real driver.

Fig. 7.a-c depict the sensed rotational motions along the *pitch*- *roll*- and *yaw*-angles during 60 to 100 seconds of motion scenario, respectively. The sensed angular velocity using the recently developed optimal WF model, classical WF and existing optimal WF model are both under the human rotational sensation treshold unit, which is necessery to prevent the DMP user from experiencing motion sickness or artefact. The translational sensation of the motion for the DMP user using three investigated techniques and the real driver are shown in Fig. 7.d-f along the longitudinal, lateral and heave channles, respectively. A better shape-following capability of the real motion signal using the proposed technique along the three linear

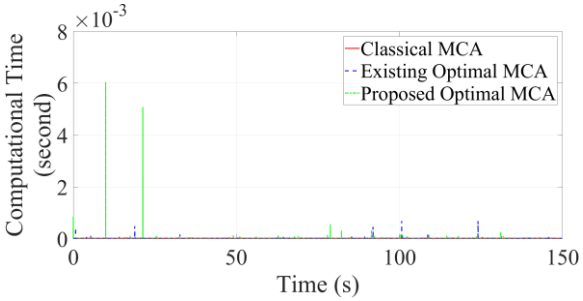


Fig. 10. The computational time of the three investigated methods including classical, existing optimal and proposed optimal WFs.

directions can be observed through the higher CC scores. This capability of the proposed optimal WF model is due to a convenient usage of the workspace boundaries via variation of the weithing matrices regarding the current DMP situation. Based on the presented results, the CC for the user of the DMP using proposed method increases 94.39% and 0.65% compared with classical and existing optimal WFs along longitudinal channel for a linear motion sensation.

The errors of the rotational motion sensation is shown in Fig. 8.a-c along the *pitch*-, *roll*- and *yaw*-angle, respectively. The RMSE difference in the rotational motion senastion between the DMP user and real vehicle driver of three investigated methods is neglibile. The errors are also under the human semicircular threshold unit. The improvement of the linear motion sensation using the recently developed technique can be noticed in Fig. 8.d-f along the *x*-, *y*- and *z*-axis, respectively. Comparing with the classical WF, the RMSE scores of the translational sensation errors yielded by the proposed technique improve by 44.15%, 42.37%, and 15.88% along the *x*-, *y*-, and *z*-axis, respectively. Also, comparing with the existing optimal WF, the RMSE scores of the translational sensation errors yielded by the proposed technique improve by 14.44%, 9.73%, and 11.73% along the x-, y-, and z-axis, respectively.

The RMSE and CC results pertaining to the regenrated motion signals using the proposed optimal WF model, the existing optimal WF model, and the classical WF model are represneted in Table III. Fig. 9.a-c depict the trasnlational displacement of the DMP using three investigated methods including the proposed optimal WF, existing optimal WF, and classical WF models along three directions in the longitudinal, lateral, and vertical channels. The proposed optimal WF model is able to better utilise the workspace boundaries than the classical and existing optimal WF model. This is owing to its ability to consider the current DMP situation, including the position and sensed error via the user to update the weighting matrices and regenrate more accurate motion signals with less false motion signals. Fig. 9.d-f show the rotational displacment of the DMP system, indicating a convenient usage of the angular workspace limitations using proposed model as compared with those of the existing model.

Finally, Fig. 10 shows the computational time of the proposed optimal WFs during the calculation of the optimal motion signal along the test using PC with the following specifications: Intel(R) Core(TM) i9-7900X CPU @ 3.30GHz 3.60 GHz with installed memory of 32.0 GB (31.7 GB usable). Based on the presented results, the computational time of the classical and existing optimal WFs are quite small as their structure is based on the constant lower and higher order transfer functions, respectively. As it is shown, the computational time of the process in all part of the motion scenario is under 0.01 seconds, which is the sampling time of the application. Then, it can be concluded that the real-time implementation of the proposed method can be handled.

The improvement of the motion sensation using the proposed optimal WF model is ascertained from the results presented in this Section. It is critical to use the workspace boundaries optimally to regenerate accurate motion signals, which can be achieved using the proposed model.

5. Conclusion

The trasnlational and rotational motions of the DMP are produced using the MCA model to respect the end-effector workspace boundries and regenrate the appropriate motion cues for the driver. In this work, the existing optimal WF model has been used as the fundamental foundation of the proposed optimal WF model with varying weighting matrices of the LQR technique. The existing optimal WF model has a set of fixed weighting matrices based on the physical DMP

limitations, including the linear displacement, linear velocity and angular displacement. The best higher order transfer function filters are extracted using the Riccati equation offline, which are employed inside the optimal WF structure to filter the motion signals (rotational velocity and translational acceleration). The proposed model is composed of NN and FLC models to solve the Riccati equation and generate the weighting matrices online inside the proposed algorithm. The Riccati equation needs the higher computational load to be solved online, and it is not feasible all the time to solve it online. As such, the NN model is trained with a data set extracted offline according to different rational weighting matrices. The trained NN model is used inside the proposed model to find the gain feedback matrix of the LQR technique and generate the optimal state space matrices. On the other hand, the FLC model is designed to generate the weighitng matrices for the NN based on the current SMBP status, including the current position and motion sensation error. The model has been developed using the MATLAB software and tuned regarding the workspace constraints of a common hexapod DMP system. The outcomes ascertain the efficacy of the proposed optimal WF model.

References

[1] J.-P. Merlet, *Parallel robots*. Springer Science & Business Media, 2006.

[2] H. Teufel, H.-G. Nusseck, K. Beykirch, J. Butler, M. Kerger, and H. Bülthoff, "MPI motion simulator: development and analysis of a novel motion simulator," in *AIAA Modeling and Simulation Technologies Conference and Exhibit*, 2007, p. 6476.

[3] T. Bellmann, J. Heindl, M. Hellerer, R. Kuchar, K. Sharma, and G. Hirzinger, "The dlr robot motion simulator part i: Design and setup," in *2011 IEEE International Conference on Robotics and Automation*, 2011: IEEE, pp. 4694-4701.

[4] S. Nahavandi, "Robot-based motion simulators using washout filtering: Dynamic, immersive land, air, and sea vehicle training, vehicle virtual prototyping, and testing," *IEEE Systems, Man, and Cybernetics Magazine*, vol. 2, no. 3, pp. 6-10, 2016.

[5] M. R. C. Qazani *et al.*, "Kinematic analysis and workspace determination of hexarot-a novel 6-DOF parallel manipulator with a rotation-symmetric arm system," *Robotica*, vol. 33, no. 8, pp. 1686-1703, 2015.

[6] M. R. C. Qazani, S. Pedrammehr, and M. J. Nategh, "An investigation on the motion error of machine tools' hexapod table," *International Journal of Precision Engineering and Manufacturing*, vol. 19, no. 4, pp. 463-471, 2018.

[7] M. R. C. Qazani, H. Asadi, S. Pedrammehr, and S. Nahavandi, "Performance analysis and dexterity monitoring of hexapod-based simulator," in *2018 4th International Conference on Control, Automation and Robotics (ICCAR)*, 2018: IEEE, pp. 226-231.

[8] J. Iskander *et al.*, "From car sickness to autonomous car sickness: A review," *Transportation research part F: traffic psychology and behaviour*, vol. 62, pp. 716-726, 2019.

[9] A. Koohestani *et al.*, "A knowledge discovery in motion sickness: a comprehensive literature review," *IEEE access*, vol. 7, pp. 85755-85770, 2019.

[10] B. Conrad and S. F. Schmidt, "A study of techniques for calculating motion drive signals for flight simulators," 1971.

[11] P. R. MacNeilage, M. S. Banks, D. R. Berger, and H. H. Bülthoff, "A Bayesian model of the disambiguation of gravitoinertial force by visual cues," *Experimental Brain Research*, vol. 179, no. 2, pp. 263-290, 2007.

[12] L. Reid and M. A. Nahon, "Flight Simulation Motion-Base Drive Algorithms.: Part 2, Selecting The System Parameters," *UTIAS report*, no. N307, 1986.

[13] L. D. Reid and M. A. Nahon, "Response of airline pilots to variations in flight simulator motion algorithms," *Journal of Aircraft*, vol. 25, no. 7, pp. 639-646, 1988.

[14] H. Asadi, A. Mohammadi, S. Mohamed, and S. Nahavandi, "Adaptive translational cueing motion algorithm using fuzzy based tilt coordination," in *International Conference on Neural Information Processing*, 2014: Springer, pp. 474-482.

[15] H. Asadi, S. Mohamed, and S. Nahavandi, "Incorporating human perception with the motion washout filter using fuzzy logic control," *IEEE/ASME Transactions on Mechatronics,* vol. 20, no. 6, pp. 3276-3284, 2015.

[16] M. R. C. Qazani, H. Asadi, M. Rostami, S. Mohamed, C. P. Lim, and S. Nahavandi, "Adaptive motion cueing algorithm based on fuzzy logic using online dexterity and direction monitoring," *IEEE Systems Journal,* 2021.

[17] M. R. C. Qazani, H. Asadi, T. Bellmann, S. Mohamed, C. P. Lim, and S. Nahavandi, "Adaptive Washout Filter Based on Fuzzy Logic for a Motion Simulation Platform with Consideration of Joints Limitations," *IEEE Transactions on Vehicular Technology,* 2020.

[18] H. Asadi, C. P. Lim, S. Mohamed, D. Nahavandi, and S. Nahavandi, "Increasing motion fidelity in driving simulators using a fuzzy-based washout filter," *IEEE Transactions on Intelligent Vehicles,* vol. 4, no. 2, pp. 298-308, 2019.

[19] M. R. C. Qazani, H. Asadi, S. Mohamed, and S. Nahavandi, "Prepositioning of a land vehicle simulation-based motion platform using fuzzy logic and neural network," *IEEE Transactions on Vehicular Technology,* vol. 69, no. 10, pp. 10446-10456, 2020.

[20] M. R. C. Qazani, H. Asadi, T. Bellmann, S. Perdrammehr, S. Mohamed, and S. Nahavandi, "A new fuzzy logic based adaptive motion cueing algorithm using parallel simulation-based motion platform," in *2020 IEEE International Conference on Fuzzy Systems (FUZZ-IEEE)*, 2020: IEEE, pp. 1-8.

[21] M. Kurosaki, "Optimal washout for control of a moving base simulator," *IFAC Proceedings Volumes,* vol. 11, no. 1, pp. 1311-1318, 1978.

[22] R. Sivan, J. Ish-Shalom, and J.-K. Huang, "An optimal control approach to the design of moving flight simulators," *IEEE Transactions on Systems, Man, and Cybernetics,* vol. 12, no. 6, pp. 818-827, 1982.

[23] M.-C. Han, H.-S. Lee, S. Lee, and M. H. Lee, "Optimal motion cueing algorithm using the human body model," *JSME International Journal Series C Mechanical Systems, Machine Elements and Manufacturing,* vol. 45, no. 2, pp. 487-491, 2002.

[24] R. J. Telban and F. M. Cardullo, "Motion cueing algorithm development: Human-centered linear and nonlinear approaches," *NASA TechReport CR-2005-213747,* 2005.

[25] W. Wu, "Development of cuing algorithms for the control of simulator motion systems," State University of New York at Binghamton, Watson School of Engineering and …, 1997.

[26] Y.-H. Chang, C.-S. Liao, and W.-H. Chieng, "Optimal motion cueing for 5-DOF motion simulations via a 3-DOF motion simulator," *Control Engineering Practice,* vol. 17, no. 1, pp. 170-184, 2009.

[27] M. Aminzadeh, A. Mahmoodi, and M. Sabzehparvar, "Optimal motion-cueing algorithm using motion system kinematics," *European Journal of Control,* vol. 18, no. 4, pp. 363-375, 2012.

[28] D. A. Pham, S. Röttgermann, F. G. Flores, and A. Kecskeméthy, "Optimal motion cueing algorithm selection and parameter tuning for sickness-free robocoaster ride simulations," in *Mechanisms, Transmissions and Applications*: Springer, 2015, pp. 127-135.

[29] H. Asadi, S. Mohamed, D. Rahim Zadeh, and S. Nahavandi, "Optimisation of nonlinear motion cueing algorithm based on genetic algorithm," *Vehicle System Dynamics,* vol. 53, no. 4, pp. 526-545, 2015.

[30] H. Asadi, S. Mohamed, C. P. Lim, and S. Nahavandi, "Robust optimal motion cueing algorithm based on the linear quadratic regulator method and a genetic algorithm," *IEEE Transactions on Systems, Man, and Cybernetics: Systems,* vol. 47, no. 2, pp. 238-254, 2016.

[31] M. R. C. Qazani, H. Asadi, and S. Nahavandi, "An Optimal Motion Cueing Algorithm Using the Inverse Kinematic solution of the Hexapod Simulation Platform," *IEEE Transactions on Intelligent Vehicles,* 2021.

[32] B. D. Anderson and J. B. Moore, *Optimal control: linear quadratic methods*. Courier Corporation, 2007.

[33] E. Lavretsky and K. A. Wise, "Optimal control and the linear quadratic regulator," in *Robust and Adaptive Control*: Springer, 2013, pp. 27-50.

[34] B. Ata and R. Coban, "Artificial bee colony algorithm based linear quadratic optimal controller design for a nonlinear inverted pendulum," *International Journal of Intelligent Systems and Applications in Engineering*, vol. 3, no. 1, pp. 1-6, 2015.

[35] M. R. C. Qazani, H. Asadi, S. Mohamed, C. P. Lim, and S. Nahavandi, "Prediction of Motion Simulator Signals Using Time-Series Neural Networks," *IEEE Transactions on Aerospace and Electronic Systems*, 2021, doi: Accepted Recently.

[36] M. R. C. Qazani, H. Asadi, M. Al-Ashmori, S. Mohamed, C. P. Lim, and S. Nahavandi, "Time Series Prediction of Driving Motion Scenarios Using Fuzzy Neural Networks:* Motion Signal Prediction Using FNNs," in *2021 IEEE International Conference on Mechatronics (ICM)*, 2021: IEEE, pp. 1-6.

[37] S. Hui and A. Goh, "Incorporating fuzzy logic with neural networks for document retrieval," *Engineering Applications of Artificial Intelligence*, vol. 9, no. 5, pp. 551-560, 1996.

[38] L. Di, T. Srikanthan, R. Chandel, and I. Katsunori, "Neural-network-based self-organized fuzzy logic control for arc welding," *Engineering applications of artificial Intelligence*, vol. 14, no. 2, pp. 115-124, 2001.

[39] N. Baklouti, A. Abraham, and A. M. Alimi, "A Beta basis function Interval Type-2 Fuzzy Neural Network for time series applications," *Engineering Applications of Artificial Intelligence*, vol. 71, pp. 259-274, 2018.

[40] D. Antanasijević, J. Antanasijević, and V. Pocajt, "Prediction of the transition temperature of bent-core liquid crystals using fuzzy “digital thermometer” model based on artificial neural networks," *Engineering Applications of Artificial Intelligence*, vol. 71, pp. 251-258, 2018.

[41] E. Bas, C. Grosan, E. Egrioglu, and U. Yolcu, "High order fuzzy time series method based on pi-sigma neural network," *Engineering Applications of Artificial Intelligence*, vol. 72, pp. 350-356, 2018.

[42] B. L. Day and R. C. Fitzpatrick, "The vestibular system," *Current biology*, vol. 15, no. 15, pp. R583-R586, 2005.

[43] H. Asadi, S. Mohamed, C. P. Lim, and S. Nahavandi, "A review on otolith models in human perception," *Behavioural brain research*, vol. 309, pp. 67-76, 2016.

[44] H. Asadi, S. Mohamed, C. P. Lim, S. Nahavandi, and E. Nalivaiko, "Semicircular canal modeling in human perception," *Reviews in the Neurosciences*, vol. 28, no. 5, pp. 537-549, 2017.

[45] I. A. Basheer and M. Hajmeer, "Artificial neural networks: fundamentals, computing, design, and application," *Journal of microbiological methods*, vol. 43, no. 1, pp. 3-31, 2000.

[46] M. H. Hassoun, *Fundamentals of artificial neural networks*. MIT press, 1995.

[47] X. Yao, "Evolving artificial neural networks," *Proceedings of the IEEE*, vol. 87, no. 9, pp. 1423-1447, 1999.

[48] B. Yegnanarayana, *Artificial neural networks*. PHI Learning Pvt. Ltd., 2009.

[49] H. J. Asl and F. Janabi-Sharifi, "Adaptive neural network control of cable-driven parallel robots with input saturation," *Engineering applications of artificial intelligence*, vol. 65, pp. 252-260, 2017.

[50] O. Elhaki and K. Shojaei, "A robust neural network approximation-based prescribed performance output-feedback controller for autonomous underwater vehicles with actuators saturation," *Engineering Applications of Artificial Intelligence*, vol. 88, p. 103382, 2020.

[51] R. M. Pattanayak, H. Behera, and S. Panigrahi, "A novel probabilistic intuitionistic fuzzy set based model for high order fuzzy time series forecasting," *Engineering Applications of Artificial Intelligence*, vol. 99, p. 104136, 2021.

[52] S. Xiang, Y. Qin, C. Zhu, Y. Wang, and H. Chen, "Long short-term memory neural network with weight amplification and its

application into gear remaining useful life prediction," *Engineering Applications of Artificial Intelligence*, vol. 91, p. 103587, 2020.

[53] S. Ghosh, A. Bandyopadhyay, S. Sahay, R. Ghosh, I. Kundu, and K. Santosh, "Colorectal Histology Tumor Detection Using Ensemble Deep Neural Network," *Engineering Applications of Artificial Intelligence*, vol. 100, p. 104202, 2021.

[54] W. Sun and C. Huang, "A carbon price prediction model based on secondary decomposition algorithm and optimized back propagation neural network," *Journal of Cleaner Production*, vol. 243, p. 118671, 2020.

[55] B. Pradhan and S. Lee, "Regional landslide susceptibility analysis using back-propagation neural network model at Cameron Highland, Malaysia," *Landslides*, vol. 7, no. 1, pp. 13-30, 2010.

[56] A. Mohammadi, S. Asadi, K. Nelson, and S. Nahavandi, "Future reference prediction in model predictive control based driving simulators," in *Australasian conference on robotics and automation (ACRA2016)*, 2016.

[57] N. Artrith and A. Urban, "An implementation of artificial neural-network potentials for atomistic materials simulations: Performance for TiO2," *Computational Materials Science*, vol. 114, pp. 135-150, 2016.